






Wearable Knee Assistive Devices for Kneeling Tasks in Construction

Siyu Chen , Duncan T. Stevenson, Shuangyue Yu , Monika Mioskowska, Jingang Yi , Hao Su , and Mitja Trkov 

Abstract—Construction workers regularly perform tasks that require kneeling, crawling, and squatting. Working in awkward kneeling postures for prolonged time periods can lead to knee pain, injuries, and osteoarthritis. In this article, we present lightweight, wearable sensing, and knee assistive devices for construction workers during kneeling and squatting tasks. Analysis of kneeling on level and sloped surfaces (0° , 10° , and 20°) is performed for single- and double-leg kneeling tasks. Measurements from the integrated inertial measurement units are used for real-time gait detection and lower limb pose estimation. Detected gait events and pose estimation are used to control the assistive knee joint torque provided by lightweight exoskeletons with powerful quasi-direct drive actuation. Human subject experiments are conducted to validate the effectiveness of the proposed analysis and control design. The results show reduction in knee extension/flexion muscle activation (up to 39%) during stand-to-kneel and kneel-to-stand tasks. Knee-ground contact forces/pressures are also reduced (up to 15%) under robotic assistance during single-leg kneeling. Increasing assistive knee torque shows redistribution of the subject's weight from the knee in contact with the ground to both supporting feet. The proposed system provides an enabling intervention to potentially reduce musculoskeletal injury risks of construction workers.

Index Terms—Construction workers, industrial exoskeletons, kneeling, wearable sensors and robots.

I. INTRODUCTION

CONSTRUCTION workers regularly perform tasks that include repetitive kneeling down/standing-up and

Manuscript received January 1, 2021; revised March 26, 2021; accepted April 29, 2021. Date of publication May 18, 2021; date of current version August 13, 2021. Recommended by Technical Editor R. Carloni and Senior Editor X. Chen. The work of Jingang Yi was supported in part by the US National Science Foundation under Grant IIS-2026613. The work of Mitja Trkov was supported by Rowan University Faculty Start-Up Fund. (Siyu Chen and Duncan Thomas Stevenson contributed equally to this work.) (Corresponding author: Mitja Trkov.)

Siyu Chen and Jingang Yi are with the Department of Mechanical and Aerospace Engineering, Rutgers University, Piscataway, NJ 08854 USA (e-mail: siyu.chen@rutgers.edu; jgyi@rutgers.edu).

Duncan T. Stevenson, Monika Mioskowska, and Mitja Trkov are with the Department of Mechanical Engineering, Rowan University, Glassboro, NJ 08028 USA (e-mail: stevensod8@students.rowan.edu; miosko82@students.rowan.edu; trkov@rowan.edu).

Shuangyue Yu and Hao Su are with the Lab of Biomechatronics and Intelligent Robotics, Department of Mechanical and Aerospace Engineering, North Carolina State University, Raleigh, NC 27695 USA (e-mail: yushuangyue0221@gmail.com; haosu.robotix@gmail.com).

Color versions of one or more figures in this article are available at <https://doi.org/10.1109/TMECH.2021.3081367>.

Digital Object Identifier 10.1109/TMECH.2021.3081367

prolonged stationary kneeling on one or both knees on flat or inclined surfaces (see Fig. 1). Roofers, HVAC mechanics, and concrete workers perform more than 66% of their working time in kneeling, crouching, stooping, crawling postures or gaits [1]. Occupational activities such as kneeling and squatting are associated with increase in knee pain, knee injuries, and knee osteoarthritis (KOA) [2]. Emerging technologies such as wearable robotics, provide promising potentials to prevent work-related musculoskeletal disorders (WMSDs) [3], [4]. All industrial exoskeletons on the market (e.g., [5]) are passive and mainly for assistance in walking, lifting, and carrying gaits that are significantly different from kneeling tasks. One of the goals of this study is to develop a wearable sensing and robotic system to assist construction workers during kneeling tasks.

Biomechanical studies have shown that static deep knee flexion kneeling alters the walking gait knee joint kinematics and kinetics, suggesting that prolonged abnormal knee loading might lead to KOA [6], [7]. Using knee savers during deep flexion kneeling was recently suggested as a potential intervention to reduce the risk of musculoskeletal disorders [8]. Distribution of forces under the knees can be modified using proper knee pads, which results in decrease of knee disorder due to kneeling [9]. Compared with walking gait, the activity of proximal muscles during kneeling is shown to increase [10]. The increased physiological demands and biomechanical loading deteriorate the comfort and lead to fatigue and injury risk of workers, which need to be minimized. Knee assistive exoskeleton can potentially reduce knee loading exposures, i.e., peak muscle activations and knee-ground contact pressures, and thus mitigate WMSD risks.

Wearable robotics is an active research field in human-robot interactions [11] and personalized technology for construction workers [12]. Real-time control of wearable robotics is challenging because of difficulty to predict human performance under dynamic variations and noises [13]. Impedance control is commonly used for human-robot interactions together with series elastic actuators (SEAs) (e.g., [14]). Instead of using SEA, quasi-direct drive (QDD) actuation was recently developed to meet the high-torque, high-backdrivability, and high-bandwidth requirements [15]–[17]. Comparing with many SEA-based robotic devices, lightweight QDD-based knee exoskeleton has demonstrated promising potentials for industrial applications.

In this article, we present a wearable mechatronic system that consists of active knee exoskeletons and a wearable sensing suite to assist construction workers in kneeling tasks. It is challenging



Fig. 1. Examples of kneeling tasks for construction workers. (a) Tile installer in double-leg kneeling. (b) Roofer in single-leg kneeling on sloped surface.

to design a lightweight exoskeleton for kneeling tasks due to large knee flexion and required high assistive power. The knee exoskeleton is adapted from the previous design [16] with extended large assistive torques without increasing additional weights and modified to wearable, nontethered configuration. We analyze the kneeling gait features on sloped surfaces. To enable real-time gait detection in kneeling tasks, a set of wearable inertial measurement units (IMUs) are used to identify various kneeling events (i.e., up, down, or stationary), types of kneeling (i.e., single- or double-leg), and kneeling with changes in trunk posture. Control of the exoskeleton device is based on the gravity compensation of the trunk and thighs to assist subject during kneeling down, standing up from kneeling position, or stationary kneeling. Human subject experiments validate the system design in assisting subject to perform required tasks. The main contributions of this work lie in the design and evaluation of the lightweight wearable sensing devices and knee exoskeletons for construction workers. New developments also include the control of the wearable device for construction workers on sloped and level surface during single- and double-leg kneeling and the feasibility demonstration of wearable assistive devices to reduce knee contact loads and muscle activation during kneeling tasks. To the authors' best knowledge, there is no reported study for use of passive or active exoskeletons in kneeling tasks. The design of flexible, lightweight, QDD-actuated exoskeleton enables feasible assistance in kneeling tasks.

The rest of this article is organized as follows. Section II introduces the wearable mechatronic devices used in this study. In Section III, we present the biomechanics model and control of exoskeleton for kneeling gaits. Experimental results and discussions are presented in Section IV. Finally, Section V summarizes the concluding remarks.

II. WEARABLE SYSTEMS FOR KNEELING TASKS

A. Wearable System Integration

We created a laboratory environment that mimicked setup of construction workers on level and sloped surfaces. Fig. 2 shows the wearable sensing and exoskeleton devices on a subject. We constructed a wooden structure with a variable surface slope and glued antiskid tape. A level surface (0°), low slope (10°), and conventional slope (20°) were used in the experiments to investigate a variety of common slopes of roof surfaces in construction [18].

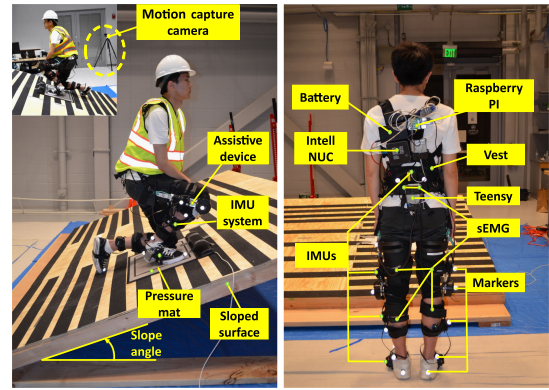


Fig. 2. Laboratory environment mimicking construction setup with variable sloped wooden structure. Wearable sensor suit and stationary sensors were used in the experiments to measure subjects' kinematics and kinetics.

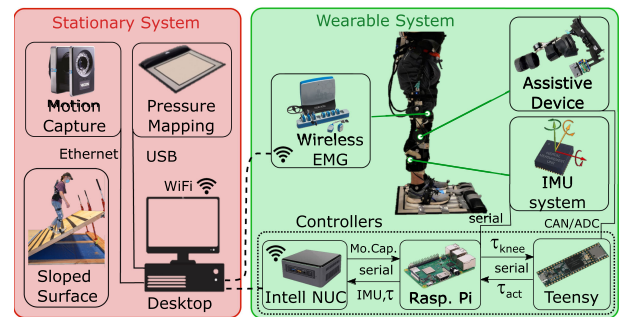


Fig. 3. Schematics of the experimental system integration. Wearable sensor suits include: bilateral knee assistive exoskeleton device, lower body IMU system, and wireless surface EMG to measure thigh, hip, and shank muscle activations. Laboratory-based stationary system consists of sloped surface with antiskid tape, optical motion capture cameras, and portable pressure mat.

Fig. 3 shows overall schematics of the wearable mechatronic systems used in the experiments. All components are connected and synchronized through desktop computer and portable high-performance microprocessor (Intel NUC7i7DNK, Intel Corporation, Santa Clara, CA, USA) through Wi-Fi wireless connection. An optical motion capture system (8 Vantage cameras, Vicon, Ltd., Oxford, U.K.) is used to collect whole body ground-truth kinematics. A portable pressure mat (MatScan, Tekscan, Inc., Boston, MA, USA) is used to measure knee/foot contact pressures on level and sloped surfaces. The wearable systems include a bilateral knee assistive exoskeleton device [16] that provides assistive torque to the individual knee, IMU system (8 units, Chordata Motion, Inc., Barcelona, Spain) to measure lower limb and trunk kinematics, and wireless surface EMG (16-channel DTS EMG, Noraxon, Inc., Scottsdale, AZ, USA) to measure human muscle activations and effort.

In the experiments, we collected data from the Vicon motion capture system at a 100-Hz sampling frequency. Sixteen reflective markers were placed on the lower limbs and trunk, and joint angles were calculated using custom algorithms in MATLAB software (MathWorks, Natick, MA, USA). Surface electrodes were placed on knee extensor muscles [rectus

femoris (RFEM), vastus lateralis (VLAT), and vastus medialis (VMED)], knee flexor muscles [biceps femoris (BFLH) and semitendinosus (SEMT)], shank extensor muscle [lateral gastrocnemius (LGAS)], and hip extensor gluteus maximus (GMAX) and hip abductor muscles [gluteus medius (GMED)]. The activations of the selected muscles were measured to evaluate the subjects' exerted effort during kneeling tasks with and without assistive torque. The EMG data were collected at 1500 Hz and the raw data were processed by a series of post-processing steps. Notch filtering (10–500 Hz) was first applied to eliminate noise. The muscle EMG activation signals were normalized with the average value of that specific muscle obtained throughout the entire trial to eliminate the effect of the applied contact pressure. The processed data were then rectified and average of root mean square was computed and used in the analysis.

B. Portable Knee Exoskeleton With QDD Actuation

The knee exoskeleton aims to assist during knee extension and distribute musculoskeletal load and stress from the knee joint to the thigh and shank. The portable knee exoskeleton design is compact by using an integrated lightweight actuator with unilateral or bilateral configuration. Fig. 4 shows the main components of the exoskeleton for unilateral configuration.

The waist belt supports the weight of the exoskeleton through elastic straps connected to the device's thigh support frame. The belt has an integrated compartment for the microcontroller and battery. The pretension of the elastic straps helps anchor the knee actuator to prevent misalignment. The thigh support frame includes a height-adjustable aluminum linkage on the lateral side of the leg, a cuff on the posterior upper thigh, and a cuff on the anterior lower thigh. The knee joint actuation system includes a QDD actuator and a customized torque sensor ($\pm 40\text{N}\cdot\text{m}$ full scale and $\pm 0.1\text{N}\cdot\text{m}$ resolution). The QDD actuator is connected to the thigh support frame, and the load cell is connected to the shank support frame. The shank support frame includes a large anterior shank cuff and a single hinge structure to provide a passive degree of freedom allowing to fit the exoskeleton to subjects of different heights. The knee exoskeleton range of motion is 0° – 160° (flexion), and the anterior lower thigh and shank contact elements do not interfere during kneeling.

The middle-sized unilateral knee exoskeleton without waist belt and battery weighed only 1.7 kg. The total weight of the bilateral knee exoskeleton (with waist belt and battery) is 4.1 kg, the lightest among reported similar devices. The overall customized QDD actuator is lightweight (710 g), compact [98 (diameter) \times 49 mm (height)], and can generate $35\text{-N}\cdot\text{m}$ peak torque. It includes a high torque density BLDC motor, a 6:1 ratio embedded planetary gear, a 16-bit high accuracy magnetic encoder, and an embedded controller. We implemented a low-level control loop for position, velocity, and current feedback. High-level control devices can send a command to read and write the real-time information through the controller area network communication protocol. The actuator can reach a nominal speed of 155 r/min (16.23 rad/s). Due to using low gear ratio transmission design, the actuator has low output inertia ($52.2\text{ kg}\cdot\text{cm}^2$), which is essential for achieving low

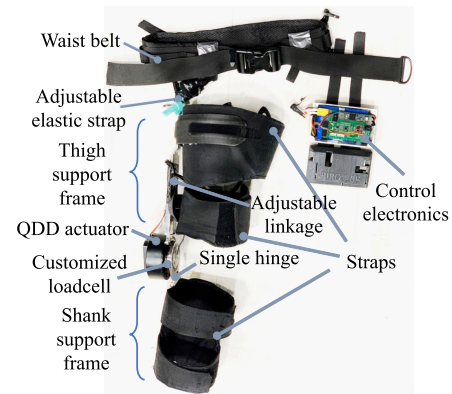


Fig. 4. Mechanism and components of the knee exoskeleton.

impedance and, therefore, minimizes the resistance to natural human movements.

The electrical system of the knee exoskeleton facilitates high-level torque control, motor control, sensor signal conditioning, data communication, and power management. The high-level microcontroller runs on Raspberry Pi and implements torque control based on the proposed torque design described in Section III. A 450-g 2500-mAh LiPo battery is used to power the knee exoskeleton, which provides over 2-h life cycle of kneeling torque assistance.

C. Experimental Protocol

Human subject tests were performed to analyze effectiveness of the device during kneeling tasks. Two healthy young male subjects ($n = 2$, age: 34 ± 4 years, mass: 75 ± 2 kg, height: 180 ± 2 cm) were recruited to perform simulated construction tasks. Only male subjects were recruited in this study, considering only 3.5% of women working in the construction and extraction occupations [19]. The testing protocol was approved by the Institutional Review Board at Rutgers University.

The main trials of the experiments included single-leg and double-leg kneeling tests. In each trial, subject performed set of kneeling tests wearing the device with three assistive torque modes: nonpowered device (“no torque”), low assistive torque (“low torque”), and high assistive torque (“high torque”), which was determined as close to maximum torque capabilities of the assistive device. Each set of tests was performed on three slopes (0° , 10° , and 20°). These specific sets of tests were designed to analyze the effect of wearing the device on muscle activation reduction during kneeling tasks. During single-leg kneeling tests, the subjects were instructed to first step on the pressure mat, stand still for 5 s, then kneel down on one knee in a kneeling position for 5 s and stand up. Seven repetitions were performed for each test. For the double-leg kneeling experiments, the subject started by standing in front of the pressure mat, then squatted down and knelt into an upright kneeling position on both knees (called Gait A), and held position for 5 s. The subject leaned forward and then backward into a full deep knee flexion position (called Gait B) and kept still in each position for 5 s. The subject then stood up simultaneously with both knees and repeated this sequence five times for each set of tests. In between

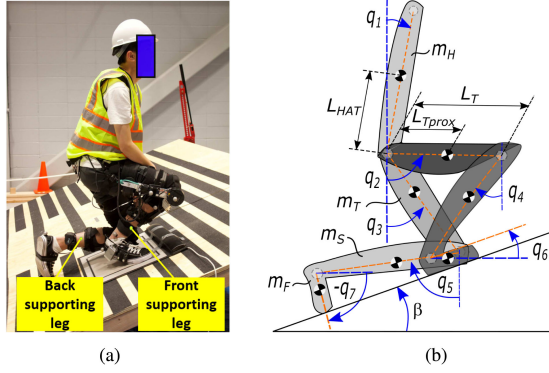


Fig. 5. (a) Construction worker during single-leg kneeling on a sloped surface. (b) Schematics of the seven-link human kneeling model. In the single-leg kneeling gaits, the back leg with knee touching the floor was defined as back supporting leg, and the other one was defined as front supporting leg.

each test set, subjects had 5-min pause to fully recover and to eliminate any fatigue effects.

III. BIPEDAL KNEELING CONTROL

A. Biomechanics Model and Knee Torque Assistance

Fig. 5 illustrates the schematic of the human biomechanics model during kneeling. Kneeling motion is considered in a sagittal plane. The human gait is represented by a seven-link rigid body model [see Fig. 5(b)]. The HAT link represents the head, arms, and torso, and is connected to both thighs. A set of relative angles q_i , $i = 1, \dots, 7$, are introduced to define the coordinates of the individual link with respect to the vertical axis for all angles except for the foot angles that are both defined with respect to the horizontal axis. Defining $\mathbf{q} = [q_1 \dots q_7]^T$ as the generalized coordinate, similar to the work in [20], the standing-to-kneeling motion dynamics are described as

$$\mathbf{D}(\mathbf{q})\ddot{\mathbf{q}} + \mathbf{C}(\mathbf{q}, \dot{\mathbf{q}})\dot{\mathbf{q}} + \mathbf{G}(\mathbf{q}) = \boldsymbol{\tau} \quad (1)$$

where $\mathbf{D}(\mathbf{q})$, $\mathbf{C}(\mathbf{q}, \dot{\mathbf{q}})$, and $\mathbf{G}(\mathbf{q})$ are the inertia, Coriolis, and gravity matrices, respectively, and $\boldsymbol{\tau}$ is the joint torque input vector. To determine the knee assistive torque during single-leg kneeling gait, as shown in Fig. 5, a quasi-static motion is considered during standing, stationary kneeling, and kneeling transitions. For construction workers, the kneeling down and standing up motions on the sloped and level surfaces are typically relatively slow, thus the assistive knee torque mainly compensates for the weight of subject's body parts along the kinematic chain between the front knee and knee contact point. We ignore the inertia and Coriolis terms in (1) and consider only gravitational terms contributions of body parts with the highest mass to obtain the estimated knee assistive torque as

$$\begin{aligned} \tau_R = & -w_R \left[m_H g (L_T \sin(q_2 + \beta) - L_H \sin(q_1 - \beta)) \right. \\ & + m_T g (L_T - L_{T_p}) \sin(q_2 + \beta) + m_T g (L_T \sin(q_2 + \beta) \\ & \left. - L_{T_p} \sin(q_3 + \beta)) \right] \quad (2) \end{aligned}$$

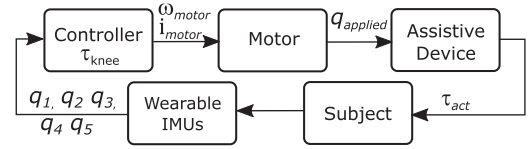


Fig. 6. Schematics of a high-level structure of controller design to provide knee assistive torques to construction workers during kneeling tasks. Thigh angles (q_2, q_3), shank angles (q_4, q_5), and low-back angle (q_1) were obtained from the IMU measurements.

where $0 \leq w_R \leq 1$ is the assistance weight factor, β is the slope angle, m_H and m_T are respectively masses of the HAT and the thigh, L_T is a length of a thigh, and L_H and L_{T_p} are distances from the hip joint to the center of mass of the HAT and thigh segments, respectively. In (2), the three terms are the moments exerted on the front supporting leg knee joint due to the gravity of the HAT, and front and back leg thighs, respectively. Although (2) is for the estimated assistance torque for the front supporting leg knee it is also used for the back supporting leg knee by swapping q_2 and q_3 due to symmetry.

The assistive torque is computed for each individual subject using their anthropometric parameters that are estimated using methods in [21]. The knee assistive torque in (2) is designed for single-leg kneeling gait. For double-leg kneeling, the last term in (2) was excluded and the torque is valid for both legs considering the respective thigh angles. This is due to the symmetric configuration of double-leg kneeling gaits and both legs equally contributing to support the weight of the subject, including HAT and thigh segments.

The amount of assistance by the exoskeleton is tuned by changing w_R in (2). The gains of torque assistance during single-leg kneeling were set as $w_R = 0.55$ and 1.00 , and $w_R = 0.4$ and 0.8 during double-leg kneeling experiments for low- and high-torque assistance, respectively. These values are chosen to prevent the torque saturation or exceeding the maximum torque capabilities of the device.

B. Exoskeleton Controller

The exoskeleton control in the previous section is primarily based on the trunk and thighs gravity compensation during kneeling gait considering upright posture as a neutral pose. Fig. 6 shows the schematics of the high-level controller design. The exoskeleton provides assistive torque to the knee joints based on the detected gait intention. The gait detection is built on the direct measurements from the wearable IMUs on thighs (q_2, q_3), shanks (q_4, q_5), and lower back (q_1). The low-level controller includes velocity feedback as an outer loop and current feedback as an inner loop to guarantee the desired torque performance and proper motion tracking of the device.

The start and end of the kneeling gait are detected based on the moving average of the last five frames (0.1 s) of the shank angle (q_4, q_5) obtained from IMU measurements. Compared to the standing pose, if the average value of shank angle exceeds a fixed threshold (i.e., 5°), the kneeling motion is detected. Similarly, if the averaged shank angle reaches again the threshold, the end of standing-up motion is detected (see Fig. 7).

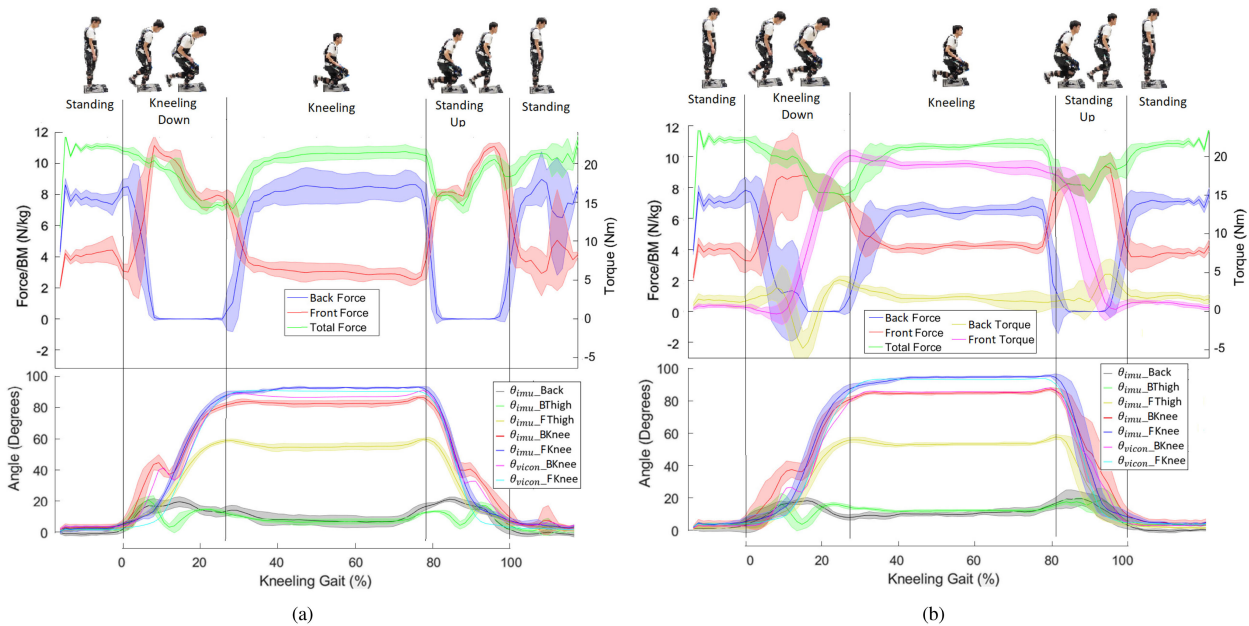


Fig. 7. Kinematics and kinetics during single-leg kneeling gait on level (0°) surface (a) without and (b) with provided “high” assistance knee torque (around $22 \text{ N} \cdot \text{m}$) during one kneeling gait. Forces were normalized with respect to the measured total force during the initial standing portion of each test set.

IV. EXPERIMENTAL RESULTS AND DISCUSSIONS

A. Experimental Results

Fig. 7 shows the ground reaction force profiles and kinematics of a representative subject during single-leg kneeling experiment on a level (0°) surface. Force profiles are normalized with respect to subjects’ body weight. The kneeling gait is defined from the beginning of the kneeling down event to the end of standing up event; see snapshots at the top of the figure. **Fig. 7(a)** shows the force profiles and kinematics without any applied assistance torque, and **Fig. 7(b)** shows the exerted high knee assistance torques and force profiles on both legs. The applied maximum mean torque (averaged over seven repetitions) is around $22 \text{ N} \cdot \text{m}$ on the knee of the front leg and close to zero torque for the knee of the other leg. Measured kinematics using the IMUs of the absolute thigh, low back, and relative knee angles show consistent trends for no, low, and high knee assistance torques. The measured contact forces under the front foot and the knee during the 50%–60% of the kneeling gait show knee load reduction [see **Fig. 7(b)**] when an assistive torque is applied to the front (right) supportive knee. The total force profiles exerted by both the front leg and knee show similar values for tests with and without torque assistance. These results confirm a weight shift from the knee on to the supporting leg under provided assistive torques.

To investigate the effect of assistance torque across various slopes, we compute and compare the average of pressure profiles during stationary kneeling period (50%–60% of the kneeling gait). **Fig. 8** shows comprehensive kinetic results from tests across all subjects on three slopes (i.e., 0° , 10° , and 20°) with three torque profiles (i.e., no, low, and high torques) for both the single- and double-leg kneeling gaits. The measured forces

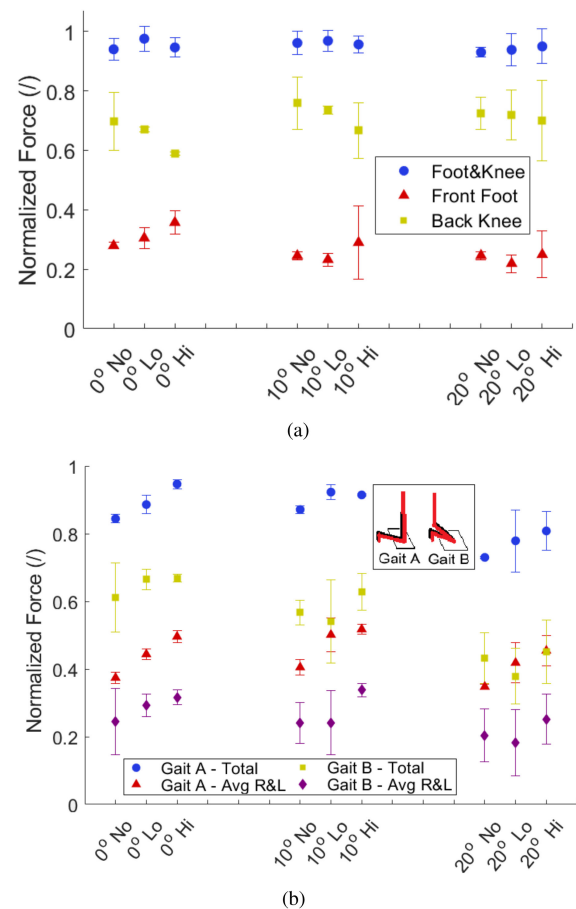


Fig. 8. Normalized knee contact forces during (a) single- and (b) double-leg kneeling gaits on 0° , 10° , and 20° sloped surfaces and various assistive torques.

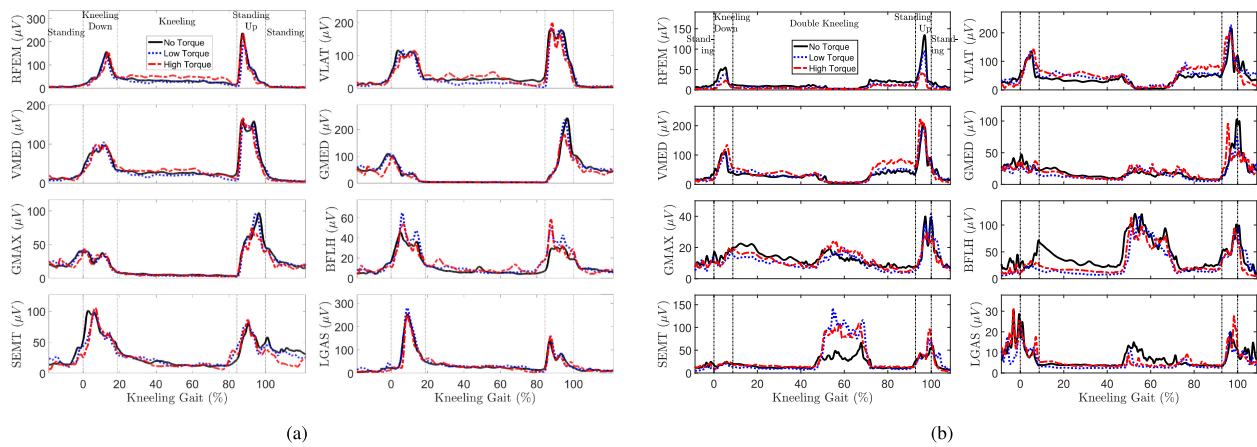


Fig. 9. Muscle activation profiles of a representative subject during (a) single-leg and (b) double-leg kneeling on a 20° sloped surface. The sEMG plots include three different assistive torque profiles: “No torque” (power OFF), “low torque,” and “high torque.” The plots are for the subject’s dominant leg, that is, front supporting leg in single-leg kneeling test. The kneeling gait is defined between the beginning of kneeling down and the ending of standing up gaits.

are normalized with respect to the total force during the initial standing portion of the individual test. The single-leg kneeling results in Fig. 8(a) show a load reduction on the knee and a load increase on the front supporting leg with the assistance torques across all surface slopes. The largest reduction (15.4%) was observed for tests on level surface with the high assistive torque. The normalized total exerted force remains constant across all tests, which implies a purely internal force redistribution due to provided assistive torque. These results suggest that the use of exoskeleton benefit in reducing knee loads applied during single-leg kneeling as potential intervention to prevent WMSD.

Fig. 8(b) shows double-leg kneeling kinetic results. An increase in the surface slope shows an overall decrease in knee contact pressure. This effect is pronounced for deep flexion kneeling (i.e., Gait B) because a significant portion of the subjects’ weight is supported by sitting back on their feet. This does not hold true for the upright double kneeling (i.e., Gait A) on the 10° sloped surface, likely because the weight of the subject’s vertical trunk is still mostly supported by the knees. The 20° slope results show a significant decrease because a much larger portion of that weight can be supported by the feet without the risk of falling forward.

Fig. 9(a) shows the EMG profiles of a representative subject’s dominant leg during single-leg kneeling gait cycle on a 20° sloped surface. Each curve represents the average value of five repetitions of the same test condition. During standing up from kneeling, the activations of knee extensor muscles (RFEM, VMED, and VLAT) of the front supporting leg are reduced under the assistive torque, compared to no torque condition. Results from both the low- and high-torque conditions show reduced muscle activations during the standing up motion. The muscle activations of hip extensor/abductor muscles (GMAX and GMED) are also reduced during the standing up stage. The peak activation of GMAX is reduced by 22.8% and the peak of GMED is reduced by 25.2% under high assistive torque. During the kneeling-down stage, the activations of knee extensor muscles remain almost the same as assistive torques increase. Fig. 9(b) shows the average muscle activations during double-leg kneeling test. Activations of knee extensors (RFEM) during kneeling

TABLE I
MUSCLE ACTIVATION CHANGES WITH EXOSKELETON FOR ALL SUBJECTS DURING SINGLE-LEG KNEELING GAIT EXPERIMENTS

Assistance	Slope	Muscles				
		RFEM	VLAT	VMED	GMED	GMAX
Low assist.	0°	-6.2%	-1.7%	-3.2%	6.4%	-2.5%
	10°	0.1%	0.5%	0.2%	2.2%	0.8%
	20°	-7.8%	-2.9%	-4.4%	-8.0%	-5.1%
High assist.	0°	-10.0%	-6.4%	-3.7%	-19.1%	-6.2%
	10°	-0.3%	-7.1%	0%	-23.8%	-5.3%
	20°	-20.5%	-18.7%	-18.4%	-39.5%	-10.9%

down and standing up are significantly reduced with increased knee assistive torques. Compared to no torque condition, the low- and high-torque conditions reduce the EMG peaks of the RFEM by 34.8% and 53.3% during the kneeling down motion and 39.5% and 55.1% for the standing up motion, respectively.

Fig. 10 shows the normalized EMG measurements during standing up portion of the single-leg [see Fig. 10(a)] and double-leg [see Fig. 10(b)] kneeling trials on three sloped surfaces. Presented box plot results show the mean, median, first and third quartile, minimum and maximum values across all subjects. Table I summarizes the muscle activation reductions, with large reductions indicated in bold. The muscle activities of knee extensors (RFEM, VMED, and VLAT) are reduced under low and high assistance torques. Compared to no assistance condition, the average muscle activities of VLAT are reduced by 6.4%, 7.1%, and 18.7% on the 0°, 10°, and 20° slopes, respectively; for RFEM, the reductions are 10.0% and 20.5% and for VMED, the reductions are 3.7% and 18.4% on the 0° and 20° slopes, respectively. On the 20° slope, the hip muscles GMED and GMAX are reduced by 39.5% and 10.9%, respectively, under high assistive torque when compared with no-torque condition. In the single-leg kneeling tests, the muscle activations of BFLH and SEMT during the standing up gait phase show an increase with the increase in surface slope. This might be due to subjects utilizing the back thigh muscles to stabilize and balance themselves on sloped surfaces. In addition, providing a high torque assistance during standing up on 0° slope

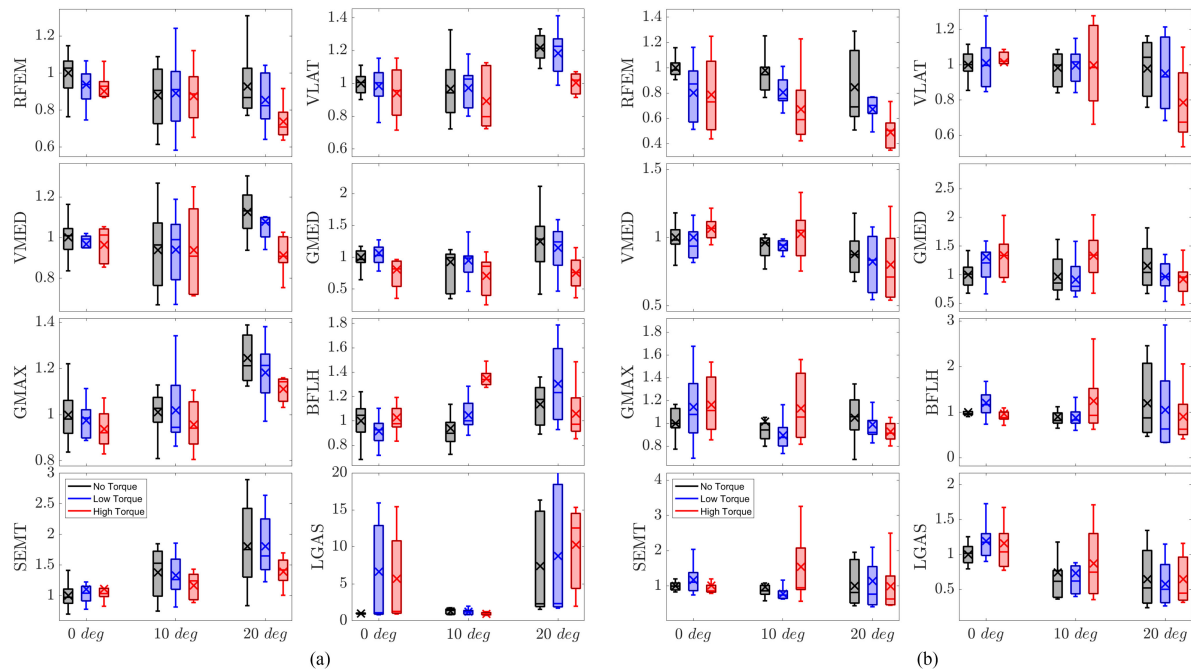


Fig. 10. Normalized EMG measurements during standing up from (a) single-leg kneeling pose and (b) double-leg deep flexion kneeling pose on three different slopes (0° , 10° , and 20°). Compared are baseline test (“no torque,” black box plots) and tests when subjects wore the device while provided two levels of assistive torque profiles (“low torque” and “high torque,” blue and red box plots, respectively). EMG profiles were normalized for individual subject to the values obtained from the baseline test (“no torque”). For each box plot, cross mark represents mean value, horizontal bar represents median value, and whiskers represents data distribution of the same muscle across all the test trials for all subjects.

shows no or minimal increase, whereas on 20° sloped surface it shows a decrease of BFLH and SEMT muscle activations compared to no torque assistance. The reason is that provided high assistive torque from a wearable device requires subjects to use less effort to stand up on sloped surface, resulting in reduced muscle cocontractions and lower muscle activations. For LGAS, the trend in muscle activation is less clear as the slope and assistive torque increase and additional investigation is required for more detailed analysis.

Fig. 10(b) shows a similar analysis for double-leg kneeling test. Under low- and high-torque assistance, the average muscle activities of knee extensor (RFEM) are reduced by 19.8%, 17.9%, 20.4% and 21.3%, 31.5%, 42.4% on the 0° , 10° , and 20° sloped surfaces, respectively. As shown in **Fig. 9(b)**, for double-leg kneeling gaits, the muscle activations of VLAT, VMED, GMED, and GMAX remain almost the same when assistive torque is applied during both kneeling down and standing up. Compared with no torque trial, the muscle activation of SEMT increased as the subject switched from upright kneeling position (Gait A) to leaning forward and backward (Gait B), whereas the muscle activation of BFLH decreased from kneeling down to Gait A. The muscle activation of VLAT and VMED slightly increased when the subjects kept the kneeling pose (during Gaits A and B) and this might be due to the adaptation to the exoskeleton. A further study is required to investigate how adaptation affects the muscle activation results.

B. Discussions

Knee angle profiles obtained from IMU measurements were compared to the ground truth results from the optical motion

capture system (see **Fig. 7**). They are in a good agreement, which validates the measurements from the wearable IMU system. The results in **Fig. 8(a)** clearly demonstrate the reduction of the exerted contact pressure on the knee when assistive knee torque is provided. This observation suggest that wearable exoskeleton can potentially reduce musculoskeletal injury risk and prevent KOA during single-leg kneeling tasks. The results of the double-leg kneeling tests in **Fig. 8(b)** show increased knee pressure with an increase of assistive torque across all slopes for Gait A kneeling. Results of Gait B deep flexion kneeling on 10° and 20° slopes show knee contact pressure decrease during low torque and increase during high torque assistance, respectively. The knee contact pressure under no assistive torque across all slopes does not show a clear correlation. Further is required to investigate the aforementioned observations.

As shown in **Table I**, activation levels of some muscles during the single-leg kneeling on the 10° sloped surface do not perfectly follow the expected trend with increased torque assistance as observed on the 0° and 20° sloped surfaces. The back thigh muscle (BFLH) shows an increased muscle activation, whereas all three knee extensor muscles (RFEM, VLAT, and VMED) show minimal changes. Further experiments are required to fully explain these results. During single-leg kneeling on 20° sloped surface, large reductions of GMED and GMAX were observed during high torque assistance compared to no torque conditions. This might be due to subjects using muscles around hips to keep postural balance on the surfaces with steep slope. The muscle activities of the back thigh and back shank muscles remained the same or slightly increased, which might be due to the imperfect fit of the device and potential misalignment between the device and the human subject. In **Fig. 9(b)**, during the 50%–70% of

the kneeling gait, the subjects were leaning forward during double-leg kneeling on 20° sloped surface. In this pose, the current configuration of the exoskeleton does not provide much assistance to the subjects. Moreover, in the forward leaning pose, the subjects utilized their back thigh muscles (i.e., SEMT) and coactivated flexor-extensor muscles to stabilize the trunk to keep their balance, thus the muscle activation increases during this process. The level of muscle activation during static leaning forward pose in double-leg kneeling needs further investigation and is part of our future work. Standing up from both single- and double-leg kneeling gaits shares similarities with squatting motion and we observed similar muscle activation increase of the knee flexors muscles (SEMT and BFLH) as previously reported during squatting task [16]. A comprehensive analysis of metabolic cost could provide additional information about the total work performed by muscles and would help evaluate benefits of using the device. Overall, using the current controller and exoskeleton design, the muscle activations during the kneeling gaits on 20° sloped surface were reduced on average by 21.6% with active control on, which indicates benefits of the exoskeleton assistance. Improved design of exoskeleton actuator and increased comfort level when wearing the exoskeleton, the assistive torque can be increased for kneeling gaits, which may result in further reduction of the muscle activations.

In our current implementation, a simplified threshold-based kneeling gait detection algorithm was used. The algorithm was sufficient for the purpose of detecting the start and end of the kneeling gait. However, the algorithm should be improved for accurate, real-time detection of complex kneeling gait events during construction tasks, which is out of the scope of this article. During kneeling tests with wearing the device, the knee and device sometimes touched the pressure mat that resulted in decrease in peak pressures. Design improvement of the device would help avoid these disturbances.

There are several limitations in this study. One is the limited number of human subjects and we need to conduct experiments on large amount of human subjects, particularly including subjects of various body sizes and ages. A specific effort will have to be made to adjust device to each individual subject to guarantee a proper fit and comfort while wearing the device. Although the results in this article demonstrate the feasibility and promising potential of the knee pressure and muscle activation reduction by supplied assistive torques, all experiments were conducted by healthy subjects and no construction workers were recruited. It would be valuable to test the wearable assistive devices with professional construction workers at industrial sites.

V. CONCLUSION

This article presented a mechatronic assistive system design in kneeling assistance for construction workers. We developed a novel controller design to assist construction workers using an improved design of a bilateral knee exoskeleton with enhanced torque capabilities (up to 35 N · m) and wearable, nontethered configuration. Several wearable and stationary sensor suites were used to measure subjects' kinetics, kinematics, and physiological parameters during kneeling tasks. The results showed

reductions in muscle activation of knee and hip extensor muscles during standing from kneeling with the highest reduction under high-torque assistance on highly sloped surfaces. Measurements of ground reaction forces showed reductions in knee pressure with increased torque assistance. The human subject testing results validated the effectiveness of the device with the goal to reduce and alleviate WMSD risk for construction workers when performing kneeling tasks on level and sloped surfaces.

REFERENCES

- [1] X. Dong, X. Wang, and R. Katz, *The Construction Chart Book—The U.S. Construction Industry and Its Workers*, 6th ed. Silver Spring, MD, USA: CPWR, 2018.
- [2] K. T. Palmer, "Occupational activities and osteoarthritis of the knee," *Brit. Med. Bull.*, vol. 102, no. 1, pp. 147–170, 2012.
- [3] J. Howard, V. V. Murashov, B. D. Lowe, and M.-L. Lu, "Industrial exoskeletons: Need for intervention effectiveness research," *Amer. J. Ind. Med.*, vol. 63, pp. 201–208, 2019.
- [4] S. Kim *et al.*, "Potential of exoskeleton technologies to enhance safety, health, and performance in construction: Industry perspectives and future research directions," *IIEE Trans. Occupat. Ergonom. Human Factors*, vol. 7, pp. 185–191, 2019.
- [5] Accessed: 2020/12/21. [Online]. Available: <http://www.suitx.com>
- [6] J. K. Hofer, R. Gejo, M. H. McGarry, and T. Q. Lee, "Effects on tibiofemoral biomechanics from kneeling," *Clin. Biomech.* vol. 26, no. 6, pp. 605–611, 2011.
- [7] T. Kajaks and P. Costigan, "The effect of sustained static kneeling on kinetic and kinematic knee joint gait parameters," *Appl. Ergonom.*, vol. 46, pp. 224–230, 2015.
- [8] S. P. Breloff *et al.*, "Are knee savers and knee pads a viable intervention to reduce lower extremity musculoskeletal disorder risk in residential roofers?" *Int. J. Ind. Ergonom.*, vol. 74, 2019, Art. no. 102868.
- [9] H. Xu, S. Jampala, D. Bloswick, J. Zhao, and A. Merryweather, "Evaluation of knee joint forces during kneeling work with different kneepads," *Appl. Ergonom.*, vol. 58, pp. 308–313, 2017.
- [10] T. Kurayama *et al.*, "A comparison of the movement characteristics between the kneeling gait and the normal gait in healthy adults," *Gait Posture*, vol. 37, no. 3, pp. 402–407, 2013.
- [11] M. Bergamasco and H. Herr, "Human-robot augmentation," in *Springer Handbook of Robotics. B. Siciliano and O. Khatib*, Eds. Berlin, Germany: Springer, 2016.
- [12] I. Awolusi, E. Marks, and M. Hallowell, "Wearable technology for personalized construction safety monitoring and trending: Review of applicable devices," *Autom. Construction*, vol. 85, pp. 96–106, 2018.
- [13] Y. Ma, X. Wu, J. Yi, C. Wang, and C. Chen, "A review on human-exoskeleton coordination towards lower limb robotic exoskeleton systems," *Int. J. Robot. Autom.*, vol. 34, no. 4, pp. 431–451, 2019.
- [14] M. K. Shepherd and E. J. Rouse, "Design and validation of a torque-controllable knee exoskeleton for sit-to-stand assistance," *IEEE/ASME Trans. Mechatronics*, vol. 22, no. 4, pp. 1695–1704, Aug. 2017.
- [15] P. M. Wensing, A. Wang, S. Seok, D. Otten, J. Lang, and S. Kim, "Proprioceptive actuator design in the MIT cheetah: Impact mitigation and high-bandwidth physical interaction for dynamic legged robots," *IEEE Trans. Robot.*, vol. 33, no. 3, pp. 509–522, Jun. 2017.
- [16] S. Yu *et al.*, "Design and control of a high-torque and highly backdrivable hybrid soft exoskeleton for knee injury prevention during squatting," *IEEE Robot. Autom. Lett.*, vol. 4, no. 4, pp. 4579–4586, Oct. 2019.
- [17] S. Yu *et al.*, "Quasi-direct drive actuation for a lightweight hip exoskeleton with high backdrivability and high bandwidth," *IEEE/ASME Trans. Mechatronics*, vol. 25, no. 4, pp. 1794–1802, Aug. 2020.
- [18] W. Johnson, *Roofers Handbook*. Carlsbad, CA, USA: Craftsman Book Company, 1976.
- [19] U. S. Bureau of Labor Statistics, "Labor force statistics from the current population survey," 2019. [Online]. Available: <https://www.bls.gov/cps/cpsaat11.htm>
- [20] M. Trkov, K. Chen, and J. Yi, "Bipedal model and extended hybrid zero dynamics of human walking with foot slips," *ASME J. Comput. Nonlinear Dyn.*, vol. 14, no. 10, 2019, Art. no. 101002.
- [21] D. A. Winter, *Biomechanics and Motor Control of Human Movement*. 2nd ed. New York, NY, USA: Wiley, 2009.